UNIVERSITÀ DEGLI STUDI DI BERGAMO
DIPARTIMENTO DI INGEGNERIA DELL'INFORMAZIONE
E METODI MATEMATICI°

QUADERNI DEL DIPARTIMENTO

Department of Information Technology and Mathematical Methods

Working Paper

Series "*Mathematics and Statistics*"

n. 7/MS – 2011

An inertia paradox for incompressible stratified Euler fluids

by

R. Camassa, S. Chen, G. Falqui, G. Ortenzi, M. Pedroni

° Viale Marconi. 5, I – 24044 Dalmine (BG), ITALY, Tel. +39-035-2052339; Fax. +39-035-562779

[§] L'accesso alle *Series* è approvato dal Comitato di Redazione. I *Working Papers* della Collana dei Quaderni del Dipartimento di Ingegneria dell'Informazione e Metodi Matematici costituiscono un servizio atto a fornire la tempestiva divulgazione dei risultati dell'attività di ricerca, siano essi in forma provvisoria o definitiva.

An inertia paradox for incompressible stratified Euler fluids

R. CAMASSA[1], S. CHEN[1], G. FALQUI[2], G. ORTENZI[2] AND M. PEDRONI[3]

[1]University of North Carolina at Chapel Hill, Carolina Center for Interdisciplinary Applied Mathematics, Department of Mathematics, Chapel Hill, NC 27599, USA
[2]Dipartmento di Matematica e Applicazioni, Università di Milano-Bicocca, Milano, Italy
[3]Dipartimento di Ingegneria dell'Informazione e Metodi Matematici, Università di Bergamo, Dalmine (BG), Italy

The interplay between incompressibility and stratification can lead to non-conservation of horizontal momentum in the dynamics of a stably stratified Euler fluid filling an infinite horizontal channel between rigid upper and lower plates. Lack of conservation occurs even though gravity is the only (vertical) force acting on the system, and no lateral boundaries are present. This apparent paradox was seemingly first noticed by Benjamin (1986) in his classification of the invariants by symmetry groups with the Hamiltonian structure of the Euler equations in two dimensional settings, but it appears to have been largely ignored since. By working directly with the motion equations, the paradox is shown here to be a consequence of the rigid lid constraint coupling through incompressibility with the infinite inertia of the far ends of the channel, assumed to be at rest in hydrostatic equilibrium. Accordingly, when inertia is removed by eliminating the stratification, or, remarkably, by using the Boussinesq approximation of uniform density for the inertia terms, horizontal momentum conservation is recovered. This interplay between constraints, incompressibility-induced action-at-a-distance and inertia is illustrated by layer averaged exact results, two-layer long-wave models, and direct numerical simulations of stratified Euler equations with smooth stratification.

1. Introduction

Among the many areas of classical mechanics, fluid dynamics arguably holds a special distinction for being a rich source of the sort of paradoxes that often arise from simplifying limit assumptions. Thus, for instance, the limit of zero viscosity gives rise to D'Alembert's paradox on the drag experienced by rigid bodies moving in ideal fluids, while the opposite limit of dominating viscous stresses leads to the Stokes or Whitehead paradoxes of unphysical divergences for the same problem.

This work focuses on an effect that could also be viewed as paradoxical: horizontal momentum conservation is violated in the dynamics of a stratified ideal fluid filling an infinite horizontal channel between rigid bottom and lid boundaries, starting from localized initial conditions, even though the only acting body-force field is the vertical gravity and the fluid is free to move laterally. Of course, even for an inviscid fluid, lateral boundaries could lead to horizontal forces by action-reaction mechanisms due to the constrained motion, and so horizontal momentum conservation cannot in general be expected to hold for a stratified Euler fluid filling a finite domain enclosed by a rigid boundary. However, we shall see below that for a domain extending horizontally to infinity the infinite inertia possessed by the far fluid at rest acts as an effective lateral boundary, giving rise to violation of horizontal momentum conservation. While stratification is

necessary for injecting inertia in the lateral fluid at rest, a subtlety of this effect is that incompressibility is also required to transmit forces arising from finite-range motion instantaneously all the way to infinity. Accordingly, the "light-cone" provided by the maximum speed of propagation of internal baroclinic modes gives a rough estimate of the boundary of the exterior region that can be considered as contributing to an effective lateral wall confinement.

To the the best of our knowledge, this limiting behaviour in the dynamics of a stratified fluid has not been given much attention in the literature. Benjamin (1986) appears to be the first to point out this curious property, in the course of his thorough investigation of the symmetries and Hamiltonian structure of the stratified, incompressible two–dimensional Euler equations. In particular, Benjamin shows that the fluid's momentum is not generally the invariant associated with translational symmetry.

While the Hamiltonian approach is compact and elegant, the physical mechanisms responsible for the dynamics seems to be more transparent by a direct approach with the simplest configuration of a two-layer fluid. This configuration has the added advantage of leading naturally into reliable models when long-wave asymptotics applies. A further advantage of the direct approach is that it can be immediately extended to three-dimensional settings for fluid domains between horizontal rigid planes. Admittedly, the effect considered here can be viewed as small, because the violation of momentum conservation scales with the size $\Delta\rho$ of the density range (which in practical cases such as water stratified with heat or salt, is typically $\Delta\rho/\rho \simeq 10^{-2}$). Of course, the effect also relies on the abstract setup of infinite rigid bounding surfaces. Nonetheless, we think that this limiting case is of conceptual importance for a proper understanding of the dynamics of the incompressible limit for density-stratified fluids.

The paper is organized as follows. In §2 we first derive balance laws that imply the paradox for incompressible stratified Euler equations in an infinite channel, without approximations. Next we show that the paradox remains in a two-layer fluid in the hydrostatic (dispersionless) non-Boussinesq approximation. In this simpler setting an explicit formula for the interface pressure can be derived. In §3, we show how the paradox can arise via direct numerical simulations of stratified incompressible Euler equations.

2. Layer averaged Euler equations

While the inertia effects we focus upon here arise with general smooth stratifications, we work first with two-layer fluids. This setup is the most convenient for developing long wave models, which can further illustrate the inertia effect by allowing explicit formulae to be derived. Similarly, the restriction to a single horizontal dimension is not essential, and our conclusions (and formalism) work for the full three-dimensional case of a horizontal fluid between infinite top and bottom rigid bounding plates. We choose to work with layer-averaged equations, which of course can be formulated independently of the assumption of stacked homogeneous layer stratification.

The dynamics of an inviscid and incompressible fluid stratified in layers of uniform density ρ_j is governed by the Euler equations for the velocity components (u_j, w_j) and the pressure p_j, in two dimensional Cartesian coordinates (x, z),

$$u_{j_x} + w_{j_z} = 0, \tag{2.1}$$

$$u_{j_t} + u_j u_{j_x} + w_j u_{j_z} = -p_{j_x}/\rho_j, \tag{2.2}$$

$$w_{j_t} + u_j w_{j_x} + w_j w_{j_z} = -p_{j_z}/\rho_j - g, \tag{2.3}$$

where g is the gravitational acceleration and subscripts with respect to space and time

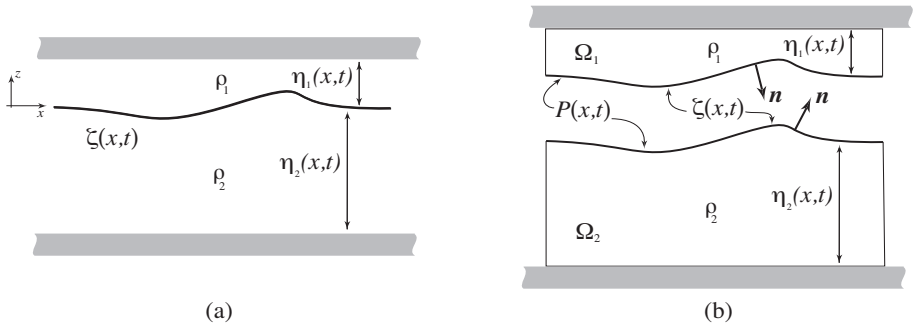

Figure 1: (a) Two-layer fluid set up and relevant notation. (b) The domains for computation of momentum balance

represent partial differentiation. In a two-fluid system, $j = 1$ ($j = 2$) stands for the upper (lower) fluid, and $\rho_1 \leq \rho_2$ must be assumed for stable stratification.

For a channel with upper and lower rigid surfaces (see figure 1a for the setup and relevant notation) the kinematic boundary conditions are

$$w_1(x, h_1, t) = 0\,, \qquad w_2(x, -h_2, t) = 0\,, \tag{2.4}$$

where h_1 (h_2) is the undisturbed thickness of the upper (lower) fluid layer, respectively. The boundary conditions at the interface $z = \zeta(x,t)$ are the continuity of normal velocity and pressure

$$\zeta_t + u_1\zeta_x = w_1, \quad \zeta_t + u_2\zeta_x = w_2, \quad p_1 = p_2 \equiv P \qquad \text{at} \quad z = \zeta(x,t), \tag{2.5}$$

where $\zeta(x,t)$ is the displacement of the interface from the equilibrium configuration surface $z = 0$ and $P(x,t)$ denotes the interfacial pressure. As to the lateral boundary conditions, a set of particular interest physically is the one that corresponds to localized initial data, i.e., the fluid is quiescent at infinity. This would require

$$\zeta(x,\cdot) \to 0\,, \quad \boldsymbol{u}_j(x,\cdot,\cdot) \to 0\,, \quad j = 1,2\,, \qquad \text{as} \quad |x| \to \infty\,, \tag{2.6}$$

sufficiently fast, which in turn implies that at infinity hydrostatic equilibrium applies,

$$p_{j\,z} + \rho_j g = 0, \quad j = 1,2\,, \qquad \Rightarrow \qquad p_j = -g\rho_j(z-\zeta) + P\,, \qquad \text{as} \quad |x| \to \infty\,. \tag{2.7}$$

In what follows we rewrite the Euler system (2.3) in terms of layer-averages (see, e.g., Camassa & Levermore, 1997). (For a smoothly stratified fluid, this is equivalent to singling out an intermediate level set of constant density $z = \zeta(x,t)$ and carrying similar manipulations since such a set will always be a material surface.) We define the layer-mean quantities $\bar{f}$ as

$$\bar{f}(x,t) \equiv \frac{1}{\eta_j}\int_{[\eta_j]} f(x,z,t)\mathrm{d}z\,, \tag{2.8}$$

where η_j are the layer-thicknesses $\eta_i \equiv h_j + (-1)^j\zeta$, and, abusing notation a little by not differentiating overbars with respect to lover or upper layer, the intervals of integration $[\eta_j]$ are $z \in (\zeta, h_1)$ for the upper- and $z \in (-h_2, \zeta)$ for the lower-layer, respectively. Vertically integrating (2.1)–(2.2) across the layers and imposing the boundary conditions

(2.4)–(2.5) yields the layer-mean equations for the upper (lower) fluid (Wu, 1981)

$$\eta_{j\,t} + \big(\eta_j \overline{u}_j\big)_x = 0, \tag{2.9}$$

$$\rho_j(\eta_j\overline{u}_j)_t + \rho_j\big(\eta_j\overline{u_j u_j}\big)_x = -(\eta_j\overline{p_j})_x + (-1)^j\zeta_x P\,, \qquad j=1,2\,. \tag{2.10}$$

(We use the notation $\overline{u_j u_j}$ here and in similar formulae below instead of the equivalent $\overline{u_j}^2$ because the latter applies only to the two dimensional case, whereas the former can be used for three dimensions as well, upon interpreting the horizontal velocity product as a two-tensor and replacing the x-derivative by a divergence over the horizontal variables.)

For incompressible, inviscid fluids under a body-force density $\boldsymbol{f}(\boldsymbol{x},t)$ in a domain Ω, the momentum balance in Eulerian form is expressed by

$$\frac{d\boldsymbol{\Pi}}{dt} \equiv \frac{d}{dt}\int_\Omega \rho\boldsymbol{u}\,dV = \int_\Omega \frac{\partial}{\partial t}(\rho\boldsymbol{u})\,dV + \int_\Omega \mathrm{div}(\rho\boldsymbol{u}\boldsymbol{u})\,dV = -\int_{\partial\Omega} p\boldsymbol{n}\,dA + \int_\Omega \rho\boldsymbol{f}\,dV\,, \tag{2.11}$$

where $\boldsymbol{n}$ is the outward normal to the surface $\partial\Omega$, and dV, dA denote the volume and area elements, respectively. Layer averages are just a local version of the integral form of the horizontal momentum balance for each layer (see figure 1b), which can be expressed by integrating equations (2.10) over some x-interval $L_- \le x \le L_+$. We have

$$\frac{d\Pi_{1\,j}}{dt} \equiv \frac{d}{dt}\int_{L_-}^{L_+}\rho_j\eta_j\overline{u}_j\,dx + \rho_j\eta_j\overline{u_j u_j}\big|_{L_-}^{L_+} = -\,\eta_j\overline{p_j}\big|_{L_-}^{L_+} + (-1)^j\int_{L_-}^{L_+}\zeta_x P\,dx\,, \tag{2.12}$$

for the upper ($j=1$) and lower ($j=2$) layer respectively, since the outward normals along the interface are $\boldsymbol{n} \propto (\pm\zeta_x, 1)$, and neither the pressure at the rigid horizontal surfaces or the external gravity field contribute horizontal components of forces.

In hydrostatic equilibrium, the layer-mean pressures are

$$\overline{p_j} = g\rho_j\frac{\eta_j}{2} + P\,, \quad j=1,2\,. \tag{2.13}$$

Hence, by a suitable definition of the limit procedure $L_\pm \to \pm\infty$, the lateral equilibrium boundary conditions imply that for each infinite upper and lower layer the horizontal momenta are conserved if and only if

$$-h_1\;P\big|_{-\infty}^{+\infty} - \int_{-\infty}^{+\infty}\zeta_x P\,dx = 0\,, \qquad -h_2\;P\big|_{-\infty}^{+\infty} + \int_{-\infty}^{+\infty}\zeta_x P\,dx = 0\,, \tag{2.14}$$

at all times, that is, if

$$\int_{-\infty}^{+\infty}\zeta_x P\,dx = 0 \qquad \text{and} \qquad P\big|_{-\infty}^{+\infty} = 0\,. \tag{2.15}$$

(These relations are precisely the ones encountered in the study of single layer fluids when an external pressure distribution is applied to their free-surface.)

Summing up the two momentum equations (2.10) (for $j=1,2$) yields the mean layer balance law for the total momentum of the fluid

$$\partial_t\Big(\rho_1(\eta_1\overline{u}_1) + \rho_2(\eta_2\overline{u}_2)\Big) = -\partial_x\Big(\rho_1\big(\eta_1\overline{u_1u_1}\big) + \rho_2\big(\eta_2\overline{u_2u_2}\big) + \eta_1\overline{p_1} + \eta_2\overline{p_2}\Big)\,. \tag{2.16}$$

By action-and-reaction the contribution from the pressure at the interface $P(x,t)$ drops from the balance (2.16) as well as from the integral version of the total horizontal momentum. Thus, the condition for total momentum conservation is that $P\big|_{-\infty}^{+\infty} = 0$, since (2.13) with (2.12) in this limit yields

$$\frac{d\Pi_1}{dt} = \frac{d\Pi_{1\,1}}{dt} + \frac{d\Pi_{1\,2}}{dt} = -(h_1+h_2)\;P\big|_{-\infty}^{+\infty}\,.$$

At first sight, for localized displacements and velocities, it might not be clear how the asymptotic values of the interfacial pressure could be different from plus to minus infinity, as the hydrostatic equilibrium is identical at both ends and the interfacial pressure simply keeps track of the overall constant of integration up to which pressure is defined. For a free upper surface, this constant is usually set by the atmospheric pressure; if this is assumed to be uniform, no pressure jump can occur. However, a system with a rigid lid is constrained, and reaction forces can develop in response to the constraint. Thus, we now focus on the consequences of the rigid lid constraint $\eta_1+\eta_2 = h_1+h_2$. The continuity equations (2.9) imply

$$\big(\eta_1\overline{u}_1 + \eta_2\overline{u}_2\big)_x = 0 \quad \Rightarrow \quad \eta_1\overline{u}_1 + \eta_2\overline{u}_2 \equiv Q(t)\,, \tag{2.17}$$

that is, the volume flux Q through the channel can only be a function of time. Dividing the momentum equations (2.10) by the respective densities and summing the resulting equations yields

$$\partial_x\Big(\eta_1\overline{u_1u_1} + \eta_2\overline{u_2u_2} + \frac{1}{\rho_1}\eta_1\overline{p_1} + \frac{1}{\rho_2}\eta_2\overline{p_2}\Big) = \Big(\frac{1}{\rho_2} - \frac{1}{\rho_1}\Big)\zeta_x P - \dot{Q}\,. \tag{2.18}$$

With the far-field zero boundary conditions on the velocities, which implies $Q(t) = 0$ at all times, equation (2.18) can be interpreted as an expression that determines the (unknown) interfacial pressure $P(x,t)$ in terms of the divergence of the layer-mean quantities. By integrating in x and taking into account the boundary conditions (2.6)-(2.7) we obtain

$$\Big(\frac{h_2}{\rho_2} + \frac{h_1}{\rho_1}\Big)\; P|_{-\infty}^{+\infty} = \Big(\frac{1}{\rho_2} - \frac{1}{\rho_1}\Big)\int_{-\infty}^{+\infty}\zeta_x P\,dx\,, \tag{2.19}$$

which shows that unless the surface integral of the pressure along the interface vanish, or the layers have the same density, the extremal values of the interfacial pressure will in general be different. The equivalent expression

$$\rho_2\Big(h_1\; P|_{-\infty}^{+\infty} + \int_{-\infty}^{+\infty}\zeta_x P\,dx\Big) = -\rho_1\Big(h_2\; P|_{-\infty}^{+\infty} - \int_{-\infty}^{+\infty}\zeta_x P\,dx\Big)$$

shows that if one of the two conditions in (2.14) is satisfied, i.e., horizontal momentum of one of the layers is conserved, the other will be as well, as the surface pressure integral is linked to the difference of asymptotic interfacial pressure by the rigid lid constraint. Thus, conservation of the horizontal momentum of just one of the two layers implies conservation of the total horizontal momentum of the fluid. On the other hand, with nonzero surface pressure integral along the interface total horizontal momentum will change with time, i.e., the bulk of the fluid will in general undergo accelerations. Notice that total horizontal momentum is always conserved if the fluid is homogeneous, $\rho_1 = \rho_2$, as (2.19) shows that in this case interfacial pressure forces cannot add up to provide a total pressure gradient between the far ends of the channel. It remains to be seen if states of the fluid leading to a nonzero interfacial integral at the right-hand of equation (2.19) can develop during the evolution governed by the Euler equations (even for a general smoothly stratified fluid). A convenient starting point is offered by a choice of initial conditions corresponding to zero velocity and a local deformation of density level sets away from the (flat) ones for hydrostatic equilibrium. This is the choice of initial data used in the numerical simulations below, where in particular we take x-antisymmetric initial deformations. As we will see, during the subsequent evolution, this choice leads to an analog for a finite domain of time-variation of horizontal momentum for the infinite channel. The numerical simulations will be performed with near two-layer configurations,

and with initial data which are slowly varying in x. For such case explicit expressions for the quantities in equation (2.19) can be derived using asymptotic approximations.

2.1. *Long wave asymptotics*

At leading order in a long-wave asymptotic expansion (see, e.g., Yih, 1980), the hydrostatic approximation for the pressures holds throughout the fluid domain, not just as far field boundary conditions. This can be used to derive a closed form expression for the interfacial pressure in equation (2.18). The result is expressed in terms of well known two-layer (five-equation, dispersionless) shallow water model (see, e.g., Milewski et al. (2004)). We have

$$\partial_x\Big(\eta_1\overline{u_1u_1}+\eta_2\overline{u_2u_2}+g\zeta h+g\frac{h_2^2-h_1^2}{2}+\Big(\frac{\eta_1}{\rho_1}+\frac{\eta_2}{\rho_2}\Big)P\Big)=\zeta_x\Big(\frac{1}{\rho_2}-\frac{1}{\rho_1}\Big)P\,,$$

so that, with the identities $\zeta_x=-\eta_{1x}=\eta_{2x}$ used in the RHS of this expression,

$$\partial_x\big(\eta_1\overline{u_1u_1}+\eta_2\overline{u_2u_2}+g\zeta h\big)=-P_x\Big(\frac{\eta_1}{\rho_1}+\frac{\eta_2}{\rho_2}\Big)\,.$$

Upon splitting the average of products into the products of averages, this coincides with the expression derived from the five-equation model, and yields

$$P|_{-\infty}^{+\infty}=-\rho_1\rho_2\int_{-\infty}^{\infty}\frac{(\eta_1\overline{u_1}^2+\eta_2\overline{u_2}^2)_x}{\rho_1\eta_2+\rho_2\eta_1}dx\,. \tag{2.20}$$

Here a term with the factor $gh\zeta_x$ has been dropped because the denominator is only a (linear) function of ζ thus making the ratio a perfect x-derivative, vanishing when the boundary conditions on ζ are applied. Thus, at leading order total horizontal momentum conservation requires the extra constraint on the choice of initial data that make the above integral vanish, which is manifestly not verified for general functions $\overline{u}_j$'s and η_j's. Note that if $\rho_1=\rho_2$ the denominator in the integrand in (2.20) becomes a constant, making the integral null on account of the velocity boundary conditions. Perhaps more notable is the effect of the Boussinesq approximation of taking $\rho_1=\rho_2$ in front of the inertial terms. Just as in the case of homogeneous density fluid, build-up of pressure jump $P|_{-\infty}^{+\infty}$ from interfacial pressure cannot occur: taking the Boussinesq approximation in, e.g., equation (2.16), and applying the constraint $Q(t)=0$ sets the right-hand side of that equation to zero, so that $\dot{\Pi}_1=0$, which in turn implies $P|_{-\infty}^{+\infty}=0$. Hence total as well as individual layer momenta are always conserved in the Boussinesq approximation for two-layer channel flows with far-field hydrostatic equilibrium boundary conditions.

Finally, we remark that equation (2.20) shows that the symmetries of the system with respect to the horizontal variable allow to identify a large class of solutions compatible with momentum conservation (in the hydrostatic approximation). Indeed, it is easy to check that if initially η_1,η_2 are even functions and $\overline{u}_1,\overline{u}_2$ are odd functions with respect to x, then these symmetries are preserved by the evolution of the system. For such solutions, (2.20) shows that the (null) horizontal momentum is conserved. However, generic initial conditions not in this class can be shown to evolve to non-zero $P|_{-\infty}^{\infty}$, even starting from null values of this pressure jump, or, remarkably, even when the velocities are chosen to be initially zero. For this latter case, this can be seen by looking at the higher order dispersive (non-hydrostatic) corrections to the shallow water model as reported in Choi & Camassa (1999). At $t=0$ with zero initial velocities these corrections modify equation (2.20) as

$$P|_{-\infty}^{+\infty}=\frac{1}{3}\int_{-\infty}^{+\infty}\frac{\big(\eta_1^3\overline{u}_{1xt}+\eta_2^3\overline{u}_{2xt}\big)_x}{\eta_1/\rho_1+\eta_2/\rho_2}\,dx\,, \tag{2.21}$$

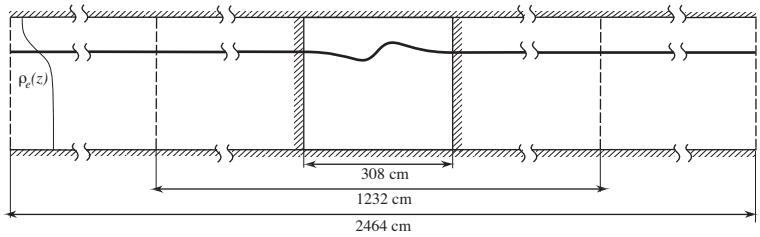

Figure 2: Sketch of the fluid test domain and its symmetrical padding by wings of increasing length, quadrupling and doubling the period as shown.

which, by bringing into the integrand the time-derivatives of the velocities shows that the pressure jump can be non-zero even if the velocities are initially zero. In particular, antisymmetric initial displacements of the interface can lead to non-zero $P|_{-\infty}^{+\infty}$, whereas this pressure jump always vanishes for symmetric initial data.

3. Numerical simulations

The above considerations have been provided with laterally unbounded domains in mind. Of course, such an idealization cannot be used either in reality or in numerical studies. Thus, we first present the (straightforward) modifications of some of the above equations for finite domains, which we will then compare with direct numerical simulations of smoothly stratified Euler flows close to the two-layer limit (that is, with relatively thin pycnoclines). The analog of equation (2.19) for a periodic domain, which requires $P|_{-L/2}^{+L/2} = 0$, becomes an equation for the time derivative of the flux,

$$\dot{Q} = -\frac{2}{L}\frac{\rho_2 - \rho_1}{\rho_2 + \rho_1}\int_{-L/2}^{+L/2} \zeta_x P \, dx \,. \tag{3.1}$$

Thus, all of the above considerations on the pressure jump can be replaced by similar ones on $\dot{Q}$, which can then be thought of as a (scaled) proxy for the pressure difference in the periodic setting.

The numerical simulations will concentrate next on this quantity as well as the horizontal momentum. Specifically, we choose a fixed-size domain of the stratified fluid, henceforth referred to as the "test section," where we will apply localized initial conditions so that the velocities and pycnocline displacements are zero at the edge of this domain. We evolve the initial data numerically for some time under both periodic and rigid vertical walls (no-flux) boundary conditions, and compute the flux Q and horizontal momentum Π_1 in this time interval. The results will then be compared with those from simulations from the same initial conditions in progressively longer channels *under periodic boundary conditions*, see figure 2. Thus, while the total horizontal momentum for these longer channels is conserved, that computed on the embedded test-section alone will in general exhibit time-dependence. Owing to the added inertia of the "padding" wings of the longer channels, we expect this time dependence to show some similarity with that of the walled-in test-section. In other words, the added inertia should act as virtual walls, which could approximate actual walls in the limit of infinite channel.

The details of our numerical simulations are as follows. The initial conditions in all our simulations (all performed using dimensional quantities, and translating the coordinates'

Figure 3: Density field from the numerical simulation of the evolution out of the initial data in the 1232 cm long tank with the center 308 cm test section marked by the small box.

origin to the bottom) are chosen to be the antisymmetric interface displacement through

$$\zeta_0(x) = h_2 + \frac{x}{2}\exp\Big(-\frac{x^2}{\sigma^2}\Big)$$

together with zero initial velocities. This function displaces the smooth equilibrium density function $\rho_e(z)$ to give the initial condition ρ_0 (with obvious meaning of notation)

$$\rho_0(x,z) = \rho_1 + \frac{\rho_2-\rho_1}{2}\left(1+\tanh\left[\gamma(\zeta_0(x)-z)\right]\right)\,, \qquad z\in[0\,,H]\,. \tag{3.2}$$

Here, $\sigma = 30$ cm, $\rho_1 = 0.999$ g/cm^3, $\rho_2 = 1.022$ g/cm^3, $H = 77$ cm, $h_2 = 62$ cm, and the thickness of the pycnocline (defined as the distance between density isolines corresponding to 10% and 90% of the total density jump) is set by the parameter $\gamma = 0.5$ to correspond to about 4.5 cm (all of these parameters are suggested by typical ones for experiments with salt-stratified water). Notice that this choice of parameters gives an error of order 10^{-10} for the departure from equilibrium at the boundary of the test-section $x = \pm 154$ cm. The simulations are performed using the numerical software VARDEN which solves the stratified incompressible Euler equations (for details see Almgren et al. (1996).) We typically use a square grid with 512 points along the vertical, although we have run tests with doubled and half this resolution to test for convergence.

Figure 4a shows the time series of the horizontal momentum of the test-section for the walled-in configuration, and compares it to that computed from quadrupled and octupled periodic extensions. As can be seen, there is indeed a tendency for the longer channel to yield a momentum evolution closer to that of the walled section, for the initial (short) time displayed. As expected, later time evolution shows larger discrepancies but still with similar overall behavior and magnitudes. This is in rough agreement with the estimate from baroclinic wave speeds, which for this parameter choice are of order 30 cm/s, and with the scales of the initial condition with respect to that of the test-section. For reference, we remark that the code maintains the total horizontal momentum for the periodic channels close to zero (the initial value) with an error of order 10^{-4}. Figure 4b presents the time series of the flux $Q(t)$ with three different channel lengths and periodic boundary conditions. The flux is computed at different x-locations, yielding the same value within an error 10^{-4} (which when used as a test, confirms the convergence of the code). As can be seen by the different curves, the flux appears to scale as the inverse of the channel length L, which can be taken as further evidence of the inertia of the padding wings acting to oppose the fluid flux (recall that in the limit of unbounded

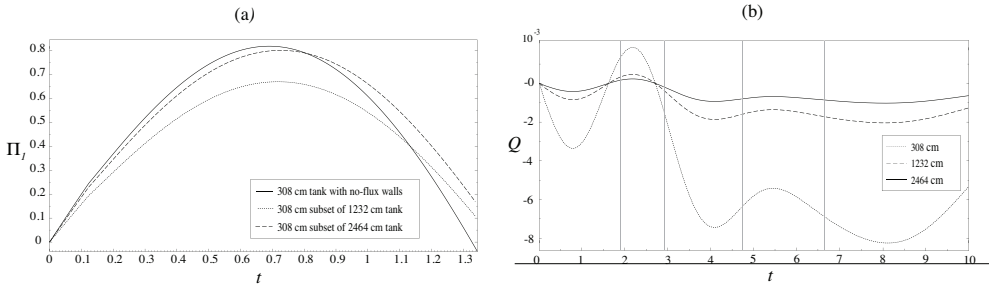

Figure 4: (a) Comparison of horizontal momentum time-evolutions for no-flux and virtual walled test section. (b) Time series of fluxes $Q(t)$ with respect to increasing period L with fixed initial conditions. The flux decreases as $1/L$ in response to the larger inertia of the padding channel wings. The thin vertical lines mark the snapshot times in figure 3.

domain $Q \equiv 0$ due to the equilibrium at infinity). The inverse scaling can be given further analytic interpretation in the long-wave approximation. In fact, the analog of (2.20) for the leading order hydrostatic (and hence dispersionless) long wave approximation is

$$\dot{Q} \int_{-L/2}^{+L/2} \frac{1}{\eta_1/\rho_1 + \eta_2/\rho_2}\, dx + \int_{-L/2}^{+L/2} \frac{(\eta_1 \overline{u_1}^2 + \eta_2 \overline{u_2}^2)_x}{\eta_1/\rho_1 + \eta_2/\rho_2}\, dx = 0\,. \tag{3.3}$$

For zero velocity initial conditions, this expression yields $\dot{Q}(0) = 0$ in contrast to the time series depicted in figure 4b. This discrepancy can remarkably be resolved by the dispersive (non-hydrostatic) terms in the strongly-nonlinear two layer model neglected in (3.3).

It is generally accepted that the dispersionless approximation works well at intermediate times, while at long times the system could display a gradient catastrophe, which can be avoided by restoring dispersive effects (Esler and Pearce (2011)). Equation (3.3) shows relevance of the dispersive effects for short times as well. From figure 4b, one can see that for the initial data we have chosen slope for the flux is initially negative, while equation (3.3) indicates that $\dot{Q}(t) = 0$ if the initial velocities are zero. As remarked above, the analog of equation (2.21) for the periodic case can improve on this model discrepancy. Specifically, at $t = 0$ with zero initial velocities the dispersive corrections turn equation (3.3) into

$$\int_{-L/2}^{+L/2} \frac{-\dot{Q}(0) + \frac{1}{3}\left(\eta_1^3 \overline{u}_{1xt} + \eta_2^3 \overline{u}_{2xt}\right)_x}{\eta_1/\rho_1 + \eta_2/\rho_2}\, dx = P|_{-L/2}^{+L/2} = 0. \tag{3.4}$$

The two-layer system (2.9) in hydrostatic approximation gives Q-dependent evolution equations for the mean layer velocities. These equations, used as a first approximation, in turn yield the value of the initial slope of the flux

$$\dot{Q}(0) = \left(\int_{-L/2}^{+L/2} \frac{B_x}{\eta_1/\rho_1 + \eta_2/\rho_2}\, dx \right) \left(\int_{-L/2}^{+L/2} \frac{1 - A_x}{\eta_1/\rho_1 + \eta_2/\rho_2}\, dx \right)^{-1}, \tag{3.5}$$

where

$$A = \frac{\eta_1^3}{3}\Big(\frac{\rho_2}{\eta_2\rho_1 + \eta_1\rho_2}\Big)_x - \frac{1}{3}\eta_2\eta_{2x}\,, \quad B = \frac{g(\rho_2 - \rho_1)\eta_1^3}{3}\Big(\frac{\eta_2\eta_{2x}}{\eta_2\rho_1 + \eta_1\rho_2}\Big)_x\,. \tag{3.6}$$

Even within this rough approximation we obtain results which are in agreement (same sign and order of magnitude) with the numerics. This can also be seen as an a posteriori

check on the robustness of the two-layer model. For instance, the theoretical prediction is $\dot{Q}(0) \simeq -1.0 \times 10^{-3}$ cm^2/s^2 for the case in figure 4b with $L = 1232$ cm, whereas the numerical result is $\dot{Q}(0) \simeq -1.8 \times 10^{-3}$ cm^2/s^2.

The above inertia effects can be further magnified by taking a larger density variation. We have carried out tests with $\rho_2 = 2\rho_1$, which should be close to the maximizer discrepancy for stratified inertia. With $\rho_2 = 1.022$ g/cm^3, the model prediction in this case is $\dot{Q}(0) \simeq -1.3$ cm^2/s^2 while the measured numerical value is $\dot{Q}(0) \simeq -1.9$ cm^2/s^2. It is likely that by taking into account the full dispersive equations (instead of just the leading order for time derivatives) the agreement could be further improved. We finally observe that the value of $\dot{Q}(0)$ obtained via (3.5) verifies the scaling $Q \sim L^{-1}$. Indeed, the only contribution to the numerator is given by the (localized) support of the η_j's, while the denominator in (3.5) possesses a term independent on the x-derivatives of the η_j's and therefore scales as L.

R.C. and S.C. gratefully acknowledge support by NSF grants DMS-0509423, DMS-1009750, RTG DMS-0943851 and CMG ARC-1025523. This work was partially supported by the MIUR Cofin2008 project *Geometrical Methods in the Theory of Nonlinear Waves and Applications*. R.C., S.C. and M.P. would like to thank the *Dipartimento di Matematica e Applicazioni* of the Milano-Bicocca University, where part of their work was done, for hospitality. We thank Paul Milewsky for sending us, while this work was being completed for submission, a preprint (Boonkasame & Milewski, 2011) on the non-Boussinesq approximation in a two-layer shallow water model with comments on the interplay between interfacial pressure and flux.

REFERENCES

Almgren A. S., Bell J. B., & Szymczak W.G. 1996 A numerical method for the incompressible Navier-Stokes equation based on an approximate projection. *J. Fluid Mech.*, **17**, 358–369.

Benjamin T. B. 1966 Internal waves of finite amplitude and permanent form. *J. Fluid Mech.*, **25**, 241–270.

Benjamin T. B. 1986 On the Boussinesq model for two-dimensional wave motions in heterogeneous fluids. *J. Fluid Mech.*, **165**, 445–474.

Boonkasame A. & Milewski P. 2011 The stability of large-amplitude shallow interfacial non-Boussinesq flows. *Stud. Appl. Math.*, DOI: 10.1111/j.1467-9590.2011.00528.x.

Camassa R. & Levermore C. D. 1997 Layer-Mean Quantities, Local Conservation Laws, and Vorticity. *Phys. Rev. Lett.*, **78**, 650–653.

Choi W. & Camassa R. 1999 Fully nonlinear internal waves in a two-fluid system. *J. Fluid Mech.*, **396**, 1–36.

Esler J. G. & Pearce J. D. 2011 Dispersive dam-break and lock-exchange flows in a two-layer fluid. *J. Fluid Mech.*, **667**, 555–585.

Long R. R. 1965 On the Boussinesq approximation and its role in the theory of internal waves. *Tellus*, **17**, 46–53.

Milewski P., Tabak E., Turner C., Rosales R.R., & Mezanque F. 2004 Nonlinear stability of two-layer flows. *Comm. Math. Sci.*, **2**, 427–442.

T. Y. Wu 1981 Long waves in ocean and coastal waters. *J. of Eng. Mech.*, **107**, 501–522.

Yih C. *Stratified Flows*, Academic Press, New York, 1980.